STAR: Structured Tokenization and Target-Aware Interest Representation for PCVR Prediction

Yimeng Xu*
Tsinghua University
Shenzhen, China
xuym24@mails.tsinghua.edu.cn

Ruihao Zhang*
Peking University
Beijing, China
2401210530@stu.pku.edu.cn

Yingqi Song*
Tsinghua University
Shenzhen, China
songyq24@mails.tsinghua.edu.cn

Ying Jiang*
Tsinghua University
Shenzhen, China
y-jiang25@mails.tsinghua.edu.cn

Lan Ma*†
Tsinghua University
Shenzhen, China
malan@sz.tsinghua.edu.cn

arXiv:2608.12986v1 [cs.IR] 13 Aug 2026

Abstract

Post-click conversion rate (PCVR) prediction is a core ranking task in industrial recommender systems. Modern ranking models must jointly capture heterogeneous non-sequential features, multi-behavior user sequences, and target-item-aware user interests, while remaining robust to high-cardinality sparse features, missing values, and train-inference inconsistencies. In this paper, we present STAR (Structured Tokenization and Target-Aware Interest Representation), a practical framework for the KDD Cup 2026 Tencent UniRec Challenge. STAR combines structured feature tokenization with target-aware interest representation on top of a HyFormer-style multi-sequence backbone. It introduces high-cardinality signal recovery, explicit user-item interaction tokens, target-aware sequence decoding, and a weighted user-item contrastive auxiliary objective inspired by InfoNCE. We further align the training and inference pipelines by reconstructing feature remapping tables and structural hyperparameters from the saved training configuration. Experiments on the challenge dataset identify the components that most reliably improve ranking AUC, while LogLoss is reported as a calibration diagnostic. The main ablation study shows a large gain from temporal context, with smaller but useful contributions from contrastive alignment, target-aware interest encoding, and high-cardinality sequence feature recovery.

Keywords

post-click conversion rate prediction, recommender systems, structured tokenization, target-aware interest representation, high-cardinality features

1 Introduction

Post-click conversion rate (PCVR) prediction estimates the probability that a user converts after interacting with a candidate item, and is typically formulated as an entire-space or post-click ranking problem [11]. It is a challenging industrial ranking task because the model must combine heterogeneous non-sequential features, sparse user/item identifiers, dense numerical signals, and multiple user behavior sequences [3, 4].

Early deep ranking models focus on explicit and implicit feature interactions, e.g., factorization machines [14], Wide&Deep [3], DeepFM [5], and DCN/DCN-V2 [19, 20]. On the sequence side, a separate line of work models user behavior histories with target attention [22, 23], self-attention sequence encoders [2, 8, 16], and search-based long-history mechanisms [10, 12]. More recent industrial ranking architectures further scale up ranking models [1, 24] and unify feature interaction with behavior sequence modeling in a single Transformer-style backbone, exemplified by HyFormer [7], MixFormer [6], and OneTrans [21]. However, in practical PCVR systems, we observe three additional challenges. First, high-cardinality sparse fields are often skipped because their embedding tables are too expensive, causing useful long-tail signals to be lost, as also observed in ultra-long history modeling [10]. Second, user sequence representations need to be conditioned on the candidate item, otherwise the extracted interest representation may be insufficiently target-aware [23]. Third, missing values, padding zeros, and feature distribution shifts can create train-inference mismatch and unstable optimization.

To address these issues, we build STAR, a framework that combines structured tokenization and target-aware interest representation on top of the provided formal baseline [7]. Our approach augments the baseline with high-cardinality feature recovery, target-aware sequence decoding, user-item interaction tokens, robust missing-value handling, and an auxiliary InfoNCE-style alignment objective [13, 17].

The main contributions are summarized as follows:

- We design a structured feature tokenization pipeline that organizes sparse IDs, dense numerical fields, temporal context, and sequence-derived signals as tokens. It also recovers high-cardinality sparse signals using cardinality capping, frequency remapping, and sequence hashing, while explicitly modeling missing values and padding zeros.
- We evaluate target-aware interest-representation enhancements, including DIN-style [23] query decoding, interest tokens, aligned sparse-dense pair pooling, and user-item non-sequential pair-product tokens.
- We introduce a weighted user-item contrastive objective inspired by InfoNCE [13, 17] and a training-inference consistency mechanism that reconstructs remapping tables and model structure during inference.

*These authors contributed equally to this work.
†Correponding author.

2 Related Work

2.1 Feature Interaction Models

Feature interaction is central to CTR and CVR prediction. Classical models use factorization [14] or cross networks [19, 20] to model low- and high-order interactions among sparse and dense fields. Hybrid architectures such as Wide&Deep [3], DeepFM [5], xDeepFM [9], and AutoInt [15] combine memorization and generalization by jointly training explicit and implicit interaction branches. More recent industrial systems adopt token-mixing or Transformer-style modules [18] to improve expressiveness under large-scale sparse feature inputs and to better exploit modern GPUs [1, 24].

2.2 Sequence Modeling for Recommendation

User behavior sequences provide important signals for preference modeling. Target attention and DIN-style activation units [22, 23], self-attention sequence encoders [8, 16], and behavior sequence Transformers [2] have been widely used to extract user interests from historical actions. To scale to ultra-long user histories under strict latency budgets, recent works explore search-based selection [12] and extremely long history modeling at web scale [10]. In PCVR prediction [11], target-aware sequence modeling is especially important because the relevant subset of history depends on the candidate item.

2.3 Unified Sequence-Feature Architectures

Recent industrial ranking models such as HyFormer [7], MixFormer [6], and OneTrans [21] seek to jointly model non-sequential features and behavior sequences within a single Transformer-style backbone. They typically tokenize heterogeneous inputs and alternate between sequence modeling and feature interaction [18], and are complementary to scaling-oriented ranking backbones such as RankMixer [24] and RankUp [1]. Our work follows this unified sequence-feature line but focuses on practical robustness for the UniRec PCVR setting, including high-cardinality feature recovery, target-aware query decoding [23], and a user-item contrastive auxiliary objective [13, 17].

3 Methodology

3.1 Problem Formulation

Let $\mathcal{U}$ and $\mathcal{I}$ denote the user and item spaces. For a user $u \in \mathcal{U}$ and a candidate item $i \in \mathcal{I}$, we observe non-sequential features $\mathbf{x}_{u,i}$ and a set of behavior sequences $\mathcal{S}_u = \{S_u^{(1)}, \ldots, S_u^{(K)}\}$. The goal is to predict the post-click conversion probability

$$\hat{y}_{u,i} = f_\theta(\mathbf{x}_{u,i}, \mathcal{S}_u), \tag{1}$$

where $y_{u,i} \in \{0, 1\}$ is the conversion label. The primary training loss is binary cross-entropy (BCE) or its focal loss variant. For standard BCE, the loss is:

$$\mathcal{L}_{\text{bce}} = -y \log \hat{y} - (1 - y) \log(1 - \hat{y}). \tag{2}$$

To address extreme class imbalance, the system defaults to using a focal loss, which introduces a modulating factor to down-weight easy examples and a class-balancing term α:

$$\mathcal{L}_{\text{focal}} = -\alpha_t (1 - p_t)^\gamma \log(p_t), \tag{3}$$

where $p_t = \hat{y}$ if $y = 1$ and $1 - \hat{y}$ otherwise, and $\alpha_t = \alpha$ if $y = 1$ and $1 - \alpha$ otherwise. We set the focusing parameter $\gamma = 2.0$ and the positive-class weight $\alpha = 0.366$ in our default configuration.

3.2 Overall Framework

Figure 1 illustrates STAR. The system contains four components: structured feature tokenization, target-aware interest representation, user-item interaction enhancement, and an auxiliary contrastive training objective.

3.3 Structured Feature Tokenization

Cardinality capping. For ultra-high-cardinality user integer fields, a full embedding table is impractical. We keep the most frequent IDs as dedicated embedding rows and fold the rare tail into a shared bucket. In this way, both specificity and commonality are effectively learned within the high-frequency IDs and the unknown category, respectively. This allows fields that would otherwise be skipped to re-enter the model with a compact trainable representation.

Frequency remapping and sequence hashing. For selected high-cardinality fields, frequent IDs are remapped to dedicated compact indices, whereas rare or unseen IDs share an unknown bucket. For sequence features that exceed the embedding threshold, we optionally route IDs through a fixed-size hash embedding branch. Thus, the features can be effectively utilized while preserving the specificity of the high-frequency features.

Missing-value and padding-zero disambiguation. Raw feature value zero can either mean a true value or padding. We therefore add non-zero masks for dense features and shift integer IDs when enabled so that padding remains index zero. Empirically, we implement zero-variance feature pruning. For fields with no variance across the dataset, instead of embedding their raw IDs, we explicitly drop their values and only extract their missing indicators, which are then projected into the model as residual dense signals. In addition, dropped features and item dense fields can emit missing indicators that are projected into the model as residual signals.

Time and meta-summary features. The model uses absolute target-time features and optional sequence periodic side information. For absolute time features at the sample-level, we select the time of day and whether on a weekend. We also compute sample-level meta summaries, such as sequence lengths, truncation ratios, recency spans, and sentinel-value statistics as our important features, and inject them into the late prediction path and query generation path.

Dense feature tokenization. As shown in Figure 2, dense features are treated as semantic continuous fields instead of being naively concatenated in our carefully designed feature pipeline. Raw Parquet float-list columns are first padded or truncated according to the schema, with missing or empty values represented by zeros. To separate real zero values from padding, selected dense blocks append a non-zero indicator mask. We then tokenize dense fields by their semantics: aligned sparse-dense pairs are used as weights for sparse multi-hot pooling, while remaining dense fields are projected into dedicated dense tokens or field-specific auxiliary tokens. These tokens are concatenated with user/item non-sequential tokens and

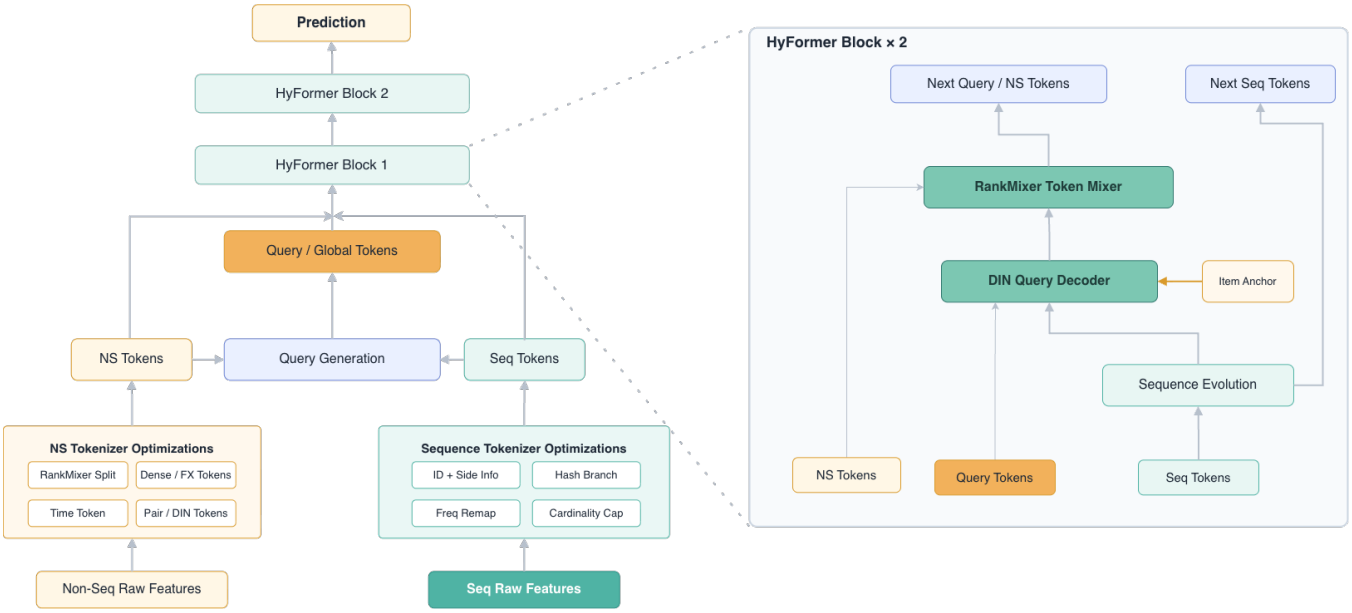

Figure 1: Overall architecture of STAR.

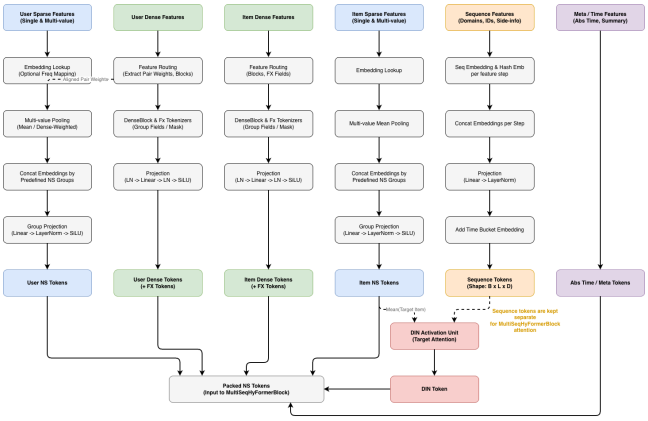

Figure 2: Structured tokenization pipeline of STAR.

sequence-derived query tokens for the final sequence-feature interaction.

3.4 Target-Aware Interest Representation

As shown in the left part of Figure 1, the backbone follows a multi-sequence HyFormer design. Non-sequential features are tokenized into user, item, dense, and auxiliary tokens. Each behavior domain is embedded into a sequence-token matrix. A query generator produces sequence-specific query tokens conditioned on non-sequential tokens and pooled sequence summaries. Unlike the formal baseline, our block uses a DIN-style query decoder. Given a sequence-specific query token $\mathbf{q}$, an item anchor $\mathbf{h}_i$, and sequence tokens $\mathbf{h}_t$, the decoder first generates a target representation $\mathbf{q}_{\text{tgt}}$ and computes attention weights α_t:

$$\mathbf{q}_{\text{tgt}} = \text{MLP}_{\text{target}}([\mathbf{q}, \mathbf{h}_i, \mathbf{q} - \mathbf{h}_i, \mathbf{q} \odot \mathbf{h}_i]) \tag{4}$$

$$\alpha_t = \text{softmax}(\text{MLP}_{\text{score}}([\mathbf{h}_t, \mathbf{q}_{\text{tgt}}, \mathbf{h}_t - \mathbf{q}_{\text{tgt}}, \mathbf{h}_t \odot \mathbf{q}_{\text{tgt}}])) \tag{5}$$

The pooled interest vector $\mathbf{z} = \sum_t \alpha_t \mathbf{h}_t$ is then used to update the query via a residual connection:

$$\mathbf{q}_{\text{out}} = \mathbf{q} + \text{MLP}_{\text{update}}([\mathbf{q}, \mathbf{z}, \mathbf{h}_i, \mathbf{q} \odot \mathbf{z}, \mathbf{h}_i \odot \mathbf{z}]) \tag{6}$$

3.5 User-Item Interaction Enhancement

We add two interaction mechanisms. First, aligned sparse-dense pair pooling uses dense values as weights over matching sparse embeddings for selected feature IDs. This avoids modeling the same signal twice and gives the model a direct weighted representation of positive pair features. Second, user and item non-sequential tokens are combined with element-wise pair-product projections, yielding explicit user-item interaction tokens. Furthermore, before feeding tokens into the HyFormer blocks, we compute an explicit target-aware interest token. Specifically, we apply a DIN activation unit over the raw sequence embeddings $\mathbf{h}_t$ anchored by the candidate item $\mathbf{h}_i$ to compute attention weights and an interest vector $\mathbf{z}$:

$$\alpha_t = \text{softmax}(g([\mathbf{h}_i, \mathbf{h}_t, \mathbf{h}_i - \mathbf{h}_t, \mathbf{h}_i \odot \mathbf{h}_t])), \quad \mathbf{z} = \sum_t \alpha_t \mathbf{h}_t \tag{7}$$

where $g(\cdot)$ is a multi-layer perceptron. We then fuse the outputs $\mathbf{z}$ across all behavior domains via an MLP, and append this fused vector as an additional non-sequential token.

3.6 Auxiliary User-Item Contrastive Objective

To align user and item representations, we project pooled user and item tokens into a shared contrastive space. For a mini-batch, the matching user-item pair is treated as the positive pair, while other

pairs act as in-batch negatives. The symmetric InfoNCE objective is

$$\mathcal{L}_{\text{nce}} = \frac{1}{2}\left[\text{CE}\left(\frac{\mathbf{U}\mathbf{V}^\top}{\tau}, \mathbf{t}\right) + \text{CE}\left(\frac{\mathbf{V}\mathbf{U}^\top}{\tau}, \mathbf{t}\right)\right], \tag{8}$$

where τ is the temperature and $\mathbf{t}$ indexes matching pairs. Converted and non-converted samples use different pair weights. The final objective is

$$\mathcal{L} = \mathcal{L}_{\text{main}} + \lambda(t)\mathcal{L}_{\text{nce}}, \tag{9}$$

where $\lambda(t)$ decays during training and is capped by the main loss ratio for stability.

3.7 Training and Inference Consistency

By using global negative sample pool, the training pipeline supports fixed global-batch manifests so that runs with different GPU counts can consume equivalent global sample sets. Regarding the data shuffle strategy, to ensure robust optimization on sequential log data, we employ a two-level buffer-based approach. We first globally shuffle the read order of data row groups, and then maintain an in-memory buffer spanning multiple batches to perform local row-level permutations. As for optimization tricks, we also use bf16 automatic mixed precision, gradient accumulation, dense-parameter EMA, and strict checkpoint sidecar files. We serialize training configurations and feature schemas during training to ensure strict alignment. Train-Inference Alignment, during inference, the dataset and model are reconstructed from the training configuration file; cardinality-cap tables and frequency mapping tables are reloaded so that the embedding layout exactly matches the trained checkpoint.

4 Experiments

We focus the experimental section on controlled single-run studies of the optimized system. We first evaluate how the model scales with hidden width, embedding dimension, and the number of HyFormer blocks, and then isolate individual modeling components through ablations. The goal is to separate capacity effects from component-level evidence and to identify which changes should be treated as optional or requiring multi-seed confirmation. Unless otherwise stated, the tables below use the full optimized default-capacity model as the reference.

4.1 Experimental Setting

Dataset and evaluation protocol. We use the KDD Cup 2026 Tencent UniRec Challenge PCVR dataset with 20000000 training samples. Each sample contains anonymized user and item identifiers, non-sequential integer and dense features, four behavior-sequence domains, a target timestamp, and a binary conversion label derived from the official label type. Unless otherwise specified, all variants use the same row-group held-out validation split and the same sequence truncation lengths (`seq_a`/`seq_b`: 256 and `seq_c`/`seq_d`: 512). The training, validation, and inference scripts rebuild feature schemas from the same configuration so that each ablation is evaluated with a consistent field order and embedding layout.

Metrics and selection. We report validation AUC, validation LogLoss, and test AUC. AUC is the primary metric because the challenge is a ranking task; LogLoss is used as a calibration diagnostic and secondary stability signal. Checkpoints are selected by validation AUC. For all ablations, ΔAUC is computed against the full optimized model, so a negative value means that removing the component hurts performance.

Implementation details. For the full system, we set $d_{\text{model}} = 128$, sparse embedding dimension to 64, the number of HyFormer blocks to 2, and the global batch size to 5880. Training uses focal loss, bf16 mixed precision, gradient accumulation, dense-parameter EMA, and a fixed global-batch manifest. The InfoNCE temperature is 0.07; its weight decays from 0.1 to 0.01 during early training and is capped relative to the main loss for stability. Unless an ablation explicitly disables a module, all variants use the same optimizer, split, sequence lengths, and checkpoint selection rule.

4.2 Full-System Reference

Table 1 compares the official baseline with the optimized full model used as the reference for all subsequent ablations. The full model (`best`) improves validation/test AUC by 0.014921/0.016585, while LogLoss is higher; we therefore keep AUC as the primary metric and use LogLoss as a calibration diagnostic. `best` configuration.

Table 1: Official baseline and full-system reference.

Model	Val AUC ↑	Test AUC ↑	Δ Test AUC
Official baseline	0.829582	0.819961	0.000000
Full optimized model	0.844503	0.836546	+0.016585

4.3 Model Scaling

Table 2 studies model capacity while keeping the same optimized training recipe and feature pipeline. Figure 3 shows the two clean dense-scaling directions. Dense-width scaling gives the clearest monotonic validation gain: increasing d_{model} from 128 to 192 and 256 raises validation AUC by 3.22 and 4.61 points in 10^{-4} units, with corresponding test AUC gains of 0.000179 and 0.000219. Depth scaling is more parameter-efficient: increasing the number of HyFormer blocks from 2 to 4 adds only 7.65M dense parameters and improves test AUC by 0.000199. In contrast, embedding-dimension scaling is less monotonic, so we discuss it separately in Appendix B.

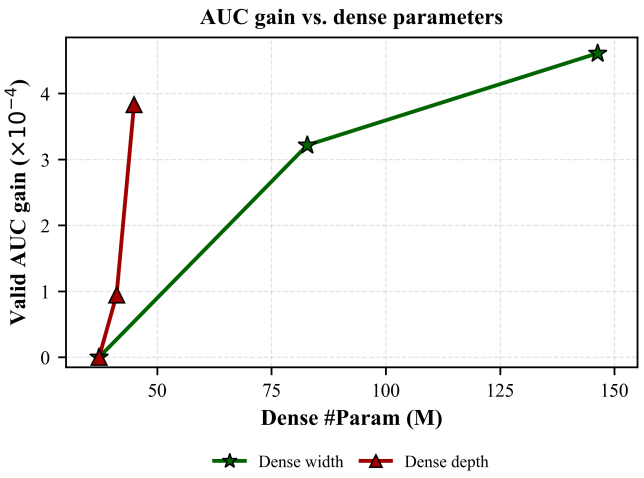

Figure 3: Validation-AUC scaling curves over dense-network parameters. The two curves isolate hidden-width scaling and block-depth scaling. Gains are measured against the default full model.

4.4 Main Modeling Ablations

Table 3 keeps only ablations whose removal lowers test AUC. This makes the main table focus on components that are supported by the current evidence, while mixed or score-increasing ablations are reported in the appendix. Temporal context is the dominant modeling contributor: removing absolute time features reduces test AUC by 0.002043. InfoNCE contributes the largest remaining modeling gain, suggesting that user-item representation alignment helps ranking even though LogLoss is not improved. DIN-based query decoding and high-cardinality sequence recovery provide smaller but consistent gains. The explicit user-item pair-product token is included because its removal is negative on test AUC, but the effect is marginal and should be confirmed with additional seeds.

4.5 Takeaways

The scaling results show that the optimized architecture benefits from additional capacity, especially hidden width and depth, but the gains are modest. The main ablation results support a complementary claim: temporal context, padding-zero disambiguation, InfoNCE alignment, DIN query decoding, and high-cardinality sequence recovery are useful modeling changes, while the pair-product token is a weak positive signal. Other modules and training-protocol choices are important engineering diagnostics, but we keep them in the appendix so that the main table does not over-claim components that are mixed, score-increasing after removal, or outside the modeling contribution.

5 Discussion

The proposed system follows a different emphasis from simply scaling a larger Transformer backbone. The formal baseline already provides a reasonable HyFormer-style architecture for mixing non-sequential features and behavior sequences. However, our empirical analysis reveals that several practical PCVR signals are missing or weakly modeled in that baseline: ultra-wide fields are skipped, zeros can be confused with padding or missing values, user histories are only weakly conditioned on the target item, and feature remapping artifacts are not treated as part of the checkpointed inference contract.

The model-scaling results make this picture more nuanced. Larger hidden width and deeper HyFormer stacks improve AUC, so part of the final system quality comes from capacity. However, scaling alone does not identify which modeling assumptions matter; the gains from dense scaling remain modest compared with the improvements from several targeted components. The ablation results make the component picture more selective. At the input level, absolute-time features are clearly important, and high-cardinality sequence recovery provides a smaller positive signal. At the interaction level, DIN-style query decoding is useful, while the explicit pair-product token is only marginal. At the objective level, weighted InfoNCE regularizes user-item representations and improves test AUC. In contrast, several plausible additions, including the fused DIN token, pair pooling, feature dropping, and meta context, improve AUC when removed in the current run. We therefore move those mixed ablations to the appendix and avoid claiming them as core contributions.

The LogLoss results also show that ranking and calibration do not move identically. The appendix shows that BCE substantially lowers validation LogLoss relative to focal loss, while focal loss keeps a small AUC advantage. We therefore treat AUC as the primary challenge metric and LogLoss as a diagnostic for calibration-sensitive deployments. Focal Loss improves ranking performance (AUC) by weighting hard samples (often the minority class), but this compromises the absolute calibration of predicted probabilities, resulting in higher LogLoss.

The main trade-off is operational complexity. Compact vocabularies, frequency maps, and hash allowlists introduce sidecar artifacts that must be versioned with the checkpoint. The fixed global-batch manifest and strict inference reconstruction mitigate this risk, but they also make the training recipe less lightweight than the formal baseline. For a final submission, components should therefore be selected by considering both their AUC/LogLoss contribution and their measured inference or maintenance cost.

This study is limited to the offline challenge setting. Unlike production-oriented ranking papers that can report online A/B tests, this work focuses on validation and leaderboard-style evaluation. The discussion should therefore be read as evidence about robust offline modeling under the released data protocol, not as a direct claim about online business metrics.

6 Conclusion

We presented STAR, a structured-tokenization and target-aware interest-representation framework for PCVR prediction in the KDD Cup 2026 Tencent UniRec Challenge. The current experiments show that the optimized architecture benefits from moderate capacity scaling, while the main ablation evidence highlights temporal context, contrastive alignment, DIN-style interest encoding, and high-cardinality sequence recovery as the most reliable modeling

Table 2: Model-scaling results. Parameter counts are shown in millions, separated into sparse embedding parameters and dense network parameters. ΔAUC is computed against the default full optimized model.

Variant	d	Emb.	Blocks	Sparse (M)	Dense (M)	Valid AUC	Valid LogLoss	Test AUC	Δ Test AUC
Default	128	64	2	333.97	37.28	0.844503	0.296215	0.836546	0.000000
Wider hidden	192	64	2	333.98	82.82	0.844825	0.295331	0.836725	+0.000179
Widest hidden	256	64	2	333.98	146.29	0.844964	0.294054	0.836765	+0.000219
Wider embedding	128	96	2	500.96	37.79	0.844906	0.295928	0.836604	+0.000058
Hidden+embedding	192	128	2	667.94	84.34	0.844736	0.295478	0.836771	+0.000225
Deeper, 3 blocks	128	64	3	333.97	41.11	0.844598	0.295587	0.836666	+0.000120
Deeper, 4 blocks	128	64	4	333.97	44.93	0.844887	0.295164	0.836745	+0.000199
Large model	192	128	4	667.94	101.53	0.844867	0.293685	0.836763	+0.000217

Table 3: Main modeling ablations whose removal lowers test AUC. ΔAUC is computed against the full optimized model.

Variant	Removed or changed component	Valid AUC	Valid LogLoss	Test AUC	Δ Test AUC
Full model	None	0.844503	0.296215	0.836546	0.000000
w/o time	Absolute target-time features	0.843018	0.298041	0.834503	-0.002043
w/o padding-zero disambiguation	Missing-value and padding-zero disambiguation	0.844606	0.295735	0.835219	-0.001327
w/o InfoNCE	Weighted user-item contrastive objective	0.844214	0.295294	0.836210	-0.000336
w/o DIN decoder	DIN+MLP query decoder replaced by cross-attention	0.844352	0.296259	0.836353	-0.000193
w/o seq hash/freq	Sequence hash embeddings and frequency remapping	0.844429	0.296518	0.836422	-0.000124
w/o UI pair-product	User/item non-sequential pair-product tokens	0.844711	0.296397	0.836514	-0.000032

contributors. Future work includes more generalized model architectures—such as UniFormer and OneTrans—that unify feature interaction and sequence modeling, while also investigating effective scaling strategies that ensure features are utilized efficiently.

Ethics and Privacy Statement

This work studies PCVR prediction using anonymized recommendation data. The proposed method does not require personally identifiable information and is intended for ranking-quality improvement under the privacy and data-use constraints of the challenge. Potential fairness and feedback loop effects should be monitored before production deployment.

References

[1] Jin Chen, Shangyu Zhang, Bin Hu, Chao Zhou, Junwei Pan, Gengsheng Xue, Wentao Ning, Gengyu Weng, Wang Zheng, Shaohua Liu, Zeen Xu, Chengyuan Mai, Shijie Quan, Tingyu Jiang, Lifeng Wang, Shudong Huang, Chengguo Yin, Haijie Gu, and Jie Jiang. 2026. RankUp: Towards High-rank Representations for Large Scale Advertising Recommender Systems. arXiv:2604.17878 [cs.IR] doi:10.48550/arXiv.2604.17878

[2] Qiwei Chen, Huan Zhao, Wei Li, Pipei Huang, and Wenwu Ou. 2019. Behavior Sequence Transformer for E-commerce Recommendation in Alibaba. In *Proceedings of the 1st International Workshop on Deep Learning Practice for High-Dimensional Sparse Data (DLP-KDD)*. 1–4. doi:10.1145/3326937.3341261

[3] Heng-Tze Cheng, Levent Koc, Jeremiah Harmsen, Tal Shaked, Tushar Chandra, Hrishi Aradhye, Glen Anderson, Greg Corrado, Wei Chai, Mustafa Ispir, Rohan Anil, Zakaria Haque, Lichan Hong, Vihan Jain, Xiaobing Liu, and Hemal Shah. 2016. Wide & Deep Learning for Recommender Systems. In *Proceedings of the 1st Workshop on Deep Learning for Recommender Systems*. 7–10. doi:10.1145/2988450.2988454

[4] Paul Covington, Jay Adams, and Emre Sargin. 2016. Deep Neural Networks for YouTube Recommendations. In *Proceedings of the 10th ACM Conference on Recommender Systems (RecSys)*. 191–198. doi:10.1145/2959100.2959190

[5] Huifeng Guo, Ruiming Tang, Yunming Ye, Zhenguo Li, and Xiuqiang He. 2017. DeepFM: A Factorization-Machine based Neural Network for CTR Prediction. In *Proceedings of the 26th International Joint Conference on Artificial Intelligence (IJCAI)*. 1725–1731. doi:10.24963/ijcai.2017/239

[6] Xu Huang, Hao Zhang, Zhifang Fan, Yunwen Huang, Zhuoxing Wei, Zheng Chai, Jinan Ni, Yuchao Zheng, and Qiwei Chen. 2026. MixFormer: Co-Scaling Up Dense and Sequence in Industrial Recommenders. Accepted by KDD 2026. arXiv:2602.14110 [cs.IR] doi:10.48550/arXiv.2602.14110

[7] Yunwen Huang, Shiyong Hong, Xijun Xiao, Jinqiu Jin, Xuanyuan Luo, Zhe Wang, Zheng Chai, Shikang Wu, Yuchao Zheng, and Jingjian Lin. 2026. HyFormer: Revisiting the Roles of Sequence Modeling and Feature Interaction in CTR Prediction. arXiv:2601.12681 [cs.IR] doi:10.48550/arXiv.2601.12681

[8] Wang-Cheng Kang and Julian McAuley. 2018. Self-Attentive Sequential Recommendation. In *2018 IEEE International Conference on Data Mining (ICDM)*. IEEE, 197–206. doi:10.1109/ICDM.2018.00035

[9] Jianxun Lian, Xiaohuan Zhou, Fuzheng Zhang, Zhongxia Chen, Xing Xie, and Guangzhong Sun. 2018. xDeepFM: Combining Explicit and Implicit Feature Interactions for Recommender Systems. In *Proceedings of the 24th ACM SIGKDD International Conference on Knowledge Discovery & Data Mining*. 1754–1763. doi:10.1145/3219819.3220023

[10] Wenhan Lyu, Devashish Tyagi, Yihang Yang, Ziwei Li, Ajay Somani, Karthikeyan Shanmugasundaram, Nikola Andrejevic, Ferdi Adeputra, Curtis Zeng, Arun K. Singh, Maxime Ransan, and Sagar Jain. 2025. DV365: Extremely Long User History Modeling at Instagram. In *Proceedings of the 31st ACM SIGKDD Conference on Knowledge Discovery and Data Mining, Volume 2*. 4717–4727. doi:10.1145/3711896.3737209

[11] Xiao Ma, Liqin Zhao, Guan Huang, Zhi Wang, Zelin Hu, Xiaoqiang Zhu, and Kun Gai. 2018. Entire Space Multi-Task Model: An Effective Approach for Estimating Post-Click Conversion Rate. In *The 41st International ACM SIGIR Conference on Research & Development in Information Retrieval*. 1137–1140. doi:10.1145/3209978.3210104

[12] Qi Pi, Guorui Zhou, Yujing Zhang, Zhe Wang, Lejian Ren, Ying Fan, Xiaoqiang Zhu, and Kun Gai. 2020. Search-based User Interest Modeling with Lifelong Sequential Behavior Data for Click-Through Rate Prediction. In *Proceedings of the 29th ACM International Conference on Information and Knowledge Management (CIKM)*. 2685–2692. doi:10.1145/3340531.3412744

[13] Alec Radford, Jong Wook Kim, Chris Hallacy, Aditya Ramesh, Gabriel Goh, Sandhini Agarwal, Girish Sastry, Amanda Askell, Pamela Mishkin, Jack Clark, Gretchen Krueger, and Ilya Sutskever. 2021. Learning Transferable Visual Models from Natural Language Supervision. In *Proceedings of the 38th International Conference on Machine Learning (Proceedings of Machine Learning Research, Vol. 139)*. 8748–8763. http://proceedings.mlr.press/v139/radford21a.html

[14] Steffen Rendle. 2010. Factorization Machines. In *2010 IEEE International Conference on Data Mining (ICDM)*. IEEE, 995–1000. doi:10.1109/ICDM.2010.127

[15] Weiping Song, Chence Shi, Zhiping Xiao, Zhijian Duan, Yewen Xu, Ming Zhang, and Jian Tang. 2019. AutoInt: Automatic Feature Interaction Learning via Self-Attentive Neural Networks. In *Proceedings of the 28th ACM International Conference on Information and Knowledge Management (CIKM)*. 1161–1170. doi:10.1145/3357384.3357925

[16] Fei Sun, Jun Liu, Jian Wu, Changhua Pei, Xiao Lin, Wenwu Ou, and Peng Jiang. 2019. BERT4Rec: Sequential Recommendation with Bidirectional Encoder Representations from Transformer. In *Proceedings of the 28th ACM International Conference on Information and Knowledge Management (CIKM)*. 1441–1450. doi:10.1145/3357384.3357895

[17] Aaron van den Oord, Yazhe Li, and Oriol Vinyals. 2018. Representation Learning with Contrastive Predictive Coding. arXiv:1807.03748 [cs.LG] doi:10.48550/arXiv.1807.03748

[18] Ashish Vaswani, Noam Shazeer, Niki Parmar, Jakob Uszkoreit, Llion Jones, Aidan N. Gomez, Łukasz Kaiser, and Illia Polosukhin. 2017. Attention is All You Need. In *Advances in Neural Information Processing Systems*, Vol. 30. 5998–6008. https://proceedings.neurips.cc/paper/2017/hash/3f5ee243547dee91fbd053c1c4a845aa-Abstract.html

[19] Ruoxi Wang, Bin Fu, Gang Fu, and Mingliang Wang. 2017. Deep & Cross Network for Ad Click Predictions. In *Proceedings of the ADKDD'17*. 12:1–12:7. doi:10.1145/3124749.3124754

[20] Ruoxi Wang, Rakesh Shivanna, Derek Cheng, Sagar Jain, Dong Lin, Lichan Hong, and Ed Chi. 2021. DCN V2: Improved Deep & Cross Network and Practical Lessons for Web-scale Learning to Rank Systems. In *Proceedings of the Web Conference 2021*. 1785–1797. doi:10.1145/3442381.3450078

[21] Zhaoqi Zhang, Haolei Pei, Jun Guo, Tianyu Wang, Yufei Feng, Hui Sun, Shaowei Liu, and Aixin Sun. 2026. OneTrans: Unified Feature Interaction and Sequence Modeling with One Transformer in Industrial Recommender. In *Proceedings of the ACM Web Conference 2026*. 8162–8170. doi:10.1145/3774904.3792838

[22] Guorui Zhou, Na Mou, Ying Fan, Qi Pi, Weijie Bian, Chang Zhou, Xiaoqiang Zhu, and Kun Gai. 2019. Deep Interest Evolution Network for Click-Through Rate Prediction. In *Proceedings of the AAAI Conference on Artificial Intelligence*, Vol. 33. 5941–5948. doi:10.1609/aaai.v33i01.33015941

[23] Guorui Zhou, Xiaoqiang Zhu, Chenru Song, Ying Fan, Han Zhu, Xiao Ma, Yanghui Yan, Junqi Jin, Han Li, and Kun Gai. 2018. Deep Interest Network for Click-Through Rate Prediction. In *Proceedings of the 24th ACM SIGKDD International Conference on Knowledge Discovery & Data Mining*. 1059–1068. doi:10.1145/3219819.3219823

[24] Jie Zhu, Zhifang Fan, Xiaoxie Zhu, Yuchen Jiang, Hangyu Wang, Xintian Han, Haoran Ding, Xinmin Wang, Wenlin Zhao, Zhen Gong, Huizhi Yang, Zheng Chai, Zhe Chen, Yuchao Zheng, Qiwei Chen, Feng Zhang, Xun Zhou, Peng Xu, Xiao Yang, Di Wu, and Zuotao Liu. 2025. RankMixer: Scaling Up Ranking Models in Industrial Recommenders. In *Proceedings of the 34th ACM International Conference on Information and Knowledge Management*. 6309–6316. doi:10.1145/3746252.3761507

Appendix

A Additional Implementation Details

The full optimized model is launched with `bash best/train/run.sh`. The default script uses RankMixer tokenization, $d_{\text{model}} = 128$, sparse embedding dimension 64, two HyFormer blocks, two query tokens per sequence, focal loss, bf16 mixed precision, dense-parameter EMA, InfoNCE temperature 0.07, and a fixed global batch size of 5880. The default sequence truncation lengths are `seq_a`/`seq_b`: 256 and `seq_c`/`seq_d`: 512. Ablations are run by changing only the removed component shown in the main and appendix ablation tables.

B Additional Sparse-Scaling Analysis

Figure 4 summarizes the embedding-size sweep, which shows a less monotonic pattern on validation. The sparse parameter count increases from 333.97M to 500.96M and then 667.94M, while validation AUC changes from 0.844503 to 0.844906 and then 0.844736. This suggests diminishing returns from simply enlarging sparse embedding tables. Test AUC does not show the same drop, but the largest embedding setting also changes d_{model} from 128 to 192, so the test gain cannot be cleanly attributed to sparse-parameter scaling alone.

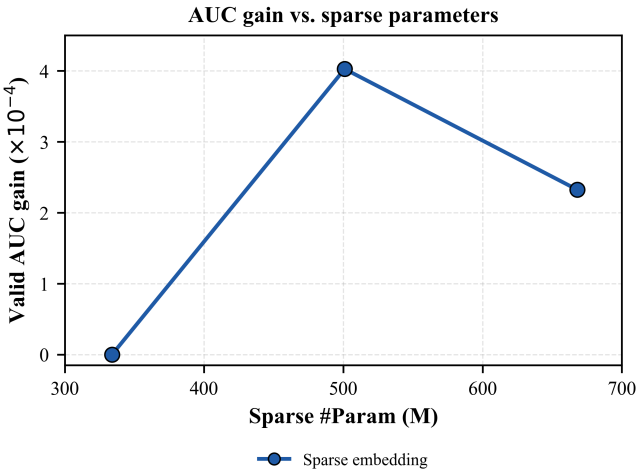

Figure 4: Validation-AUC scaling curve over sparse embedding parameters. The last point also changes d_{model} from 128 to 192, so it should be interpreted as a mixed sparse-and-dense capacity setting.

C Additional Ablations

Table 4 reports modeling ablations whose removal does not hurt test AUC in the current single-run setting. These modules are therefore not included in the main ablation table. They remain useful diagnostics because they indicate which additions may be redundant, seed-sensitive, or over-specialized to the validation split.

Table 4: Mixed modeling ablations moved out of the main table.

Variant	Removed or changed component	Val AUC	LogLoss	Test AUC	Δ Test AUC
Full model	None	0.844503	0.296215	0.836546	0.000000
w/o DIN token	Fused target-aware interest token	0.844496	0.295950	0.836587	+0.000041
w/o pair pooling	Weighted sparse-dense pooling for aligned pair fields	0.844724	0.296050	0.836651	+0.000105
w/o drop 89–91	Keep user integer fields 89–91 and remove their missing residual	0.844632	0.295822	0.836662	+0.000116
w/o meta context	Disable stage-2 meta summary and stage-3 query conditioning	0.844516	0.296400	0.836650	+0.000104

Table 5 reports training-protocol ablations. These results are important for reproducing the final system but are kept separate from the main modeling table because they evaluate optimization and data-ordering choices rather than architectural components.

Table 5: Training-protocol ablations.

Variant	Removed or changed component	Val AUC	LogLoss	Test AUC	Δ Test AUC
Full model	None	0.844503	0.296215	0.836546	0.000000
w/o EMA	Disable dense-parameter EMA checkpoint selection	0.842331	0.290766	0.834403	-0.002143
w/o shuffle	Remove the shuffle strategy	0.843950	0.297668	0.835849	-0.000697
BCE loss	Replace focal loss with BCE	0.844348	0.212041	0.836411	-0.000135

D Failed Attempts and Analysis

In this section, we will discuss the modifications that were effective in the preliminary round but ineffective in the final round, as well as some individual modifications that were effective in both rounds but could not be combined.

D.1 Modifications Effective In The Preliminary Round But Ineffective In The Final Round

The first part concerns modifications effective in the preliminary round but ineffective in the final round.

This primarily involves adversarial training with FSGM, which showed some improvement in the preliminary round. This was partly due to the smaller size of the preliminary dataset compared to the final round, posing a risk of overfitting. Adversarial training effectively mitigated this problem. However, in the final round, FSGM could not be consistently integrated into the main solution.

Regarding temporal features, the strategy used in the preliminary round could not be effectively integrated; this was because the preliminary round's approach incorporated a discrete "day-of-week" feature, and the resulting embedding introduced noise during the semi-final round due to differences in the test data distribution.

In addition, we observed a clear data-scale-dependent preference in the choice of sequence encoder. In the preliminary stage, the Transformer-based sequence encoder performed better, whereas in the final stage, the attention-free SwiGLU encoder achieved superior performance. Since the amount of training data in the preliminary stage was only about 1/19 of that in the final stage, this result suggests that the effectiveness of a sequence encoder depends not only on its modeling capacity, but also on the available data scale and computational budget. This phenomenon indicates a data-scale-driven architectural transition: in the small-data regime, Transformer benefits from its stronger sequential inductive bias; in the large-data regime, SwiGLU becomes preferable due to its efficiency, implicit regularization effect, and clearer division of labor with downstream target-aware interaction modules.

D.2 Partially Effective But Difficult To Combine

The second part consists of changes that are partially effective, but difficult to integrate. These include changing the dense compression from a single token to 2-5 tokens and the utilization of the item id.

Expanding the dense representation from a single token to multiple tokens works on the baseline individually, but fails in the final ensemble. This expansion likely disrupts the compression bottleneck, increasing the risk of overfitting.

Using item IDs, especially with unknown tokens, is only effective under certain dropout ratios during training; it may have negative benefits under other hyperparameters.

D.3 Better Along The Way, Worse In The Final Solution

There were improvements along the way, but points were lost when the final solution could not be achieved.

On the one hand, calculate an additional global Target-aware interest token and concatenate it to the NS Tokens. Because DINMLP-QueryDecoder already gives all Sequence Queries strong Target-aware capabilities, adding an extra global DIN Token introduces information redundancy, potentially diluting the attention of other features in the RankMixer Block.

On the other hand, extract meta features such as sequence length, truncation rate, and time span and add them to the prediction. It is prone to overfitting to specific splits of the validation set. In scenarios where there is a distribution shift in train-inference, meta features are often most susceptible to shift, leading to dropped test set data.

D.4 Other Failed Attempts Summary

In addition, we conducted numerous experiments, trying various methods for generating queries using different windows and long sequence modeling (e.g., longer), but without achieving significant gains. These results are related to the distribution of the data and the regularization strength of the proposed solution.

Other interesting points include the fact that removing some invalid features may decrease the value but increase the test result, which could be due to reducing the likelihood of overfitting.

An important observation during the competition was that while certain architectural changes appeared locally optimal at specific stages, they were not globally optimal in the final ensemble.

Another key finding is that the benefits of scaling up rely on proper feature handling and a sufficient volume of data. Our attempts to scale up during the competition were premature; at that stage, we had not adequately addressed feature processing, which made the models highly prone to overfitting and resulted in significant deficiencies in how capacity was allocated to utilize each effective feature. Consequently, our approach failed to effectively

scale up while simultaneously resolving the issues of feature processing and utilization.